THE JOURNAL OF PHYSICAL CHEMISTRY Letters

Letter

pubs.acs.org/JPCL

Decaheme Cytochrome MtrF Adsorption and Electron Transfer on Gold Surface

Tao Wei,*[,†] Heng Ma,[†] and Aiichiro Nakano*[,‡,§,∥,⊥]

[†]Dan F. Smith Department of Chemical Engineering, Lamar University, Beaumont, Texas 77710, United States

[‡]Department of Computer Science, University of Southern California, Los Angeles, California 90089-0781, United States

[§]Department of Physics and Astronomy, University of Southern California, Los Angeles, California 90089-0484, United States

[∥]Molecular and Computational Biology Section, Department of Biological Sciences, University of Southern California, Los Angeles, California 90089-0371, United States

[⊥]Mork Family Department of Chemical Engineering and Materials Science, University of Southern California, Los Angeles, California 90089-1211, United States

Supporting Information

ABSTRACT: Emergent electrical properties of multiheme cytochromes have promising applications. We performed hybrid simulations (molecular dynamics, free energy computation, and kinetic Monte Carlo) to study decaheme cytochrome, MtrF adsorption on an Au (111) surface in water and the electron transfer (ET) efficiency. Our results reveal that the gold surface's dehydration serves as a crucial driving force for protein adsorption due to large surface tension. The most possible adsorption orientation is with the ET terminal (heme5) approaching the gold surface, which yields a pathway for ET between the substrate and the aqueous environment. Upon adsorption, protein's secondary structures and central domains (II and IV) bonded with heme-residues remain relatively stable. MtrF surface mobility is dictated by thiol-gold interaction and strong binding between Au(111) and peptide aromatic groups. ET transfer rate across protein heme-network along the solvent-to-surface direction is slightly larger than that of the reverse direction, but lower than that of the solvation structure.

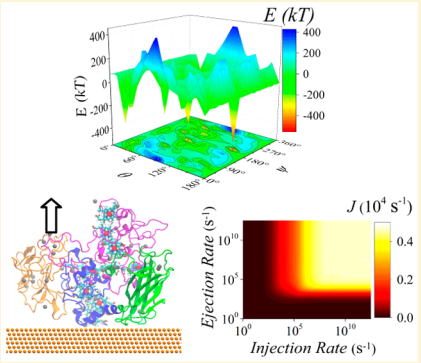

Reduction and oxidation (redox) reactions govern a variety of biological energy-conversion processes, including respiration.[1] Electron transfer (ET) within and across biological molecules is a key process that essentially dictates biological redox reactions. Heme is one of the most prevalent cofactors in nature and displays significant biological functionalities related to redox and ET processes. Cytochromes form a large family of proteins, most of which contain *c*-type heme, namely, irons coordinated by protoporphyrin IX covalently linked to the peptide by thioether bonds.[2] Multiheme cytochromes have two, or even more, *c*-type hemes with the irons' neighboring distance less than 1.55 nm.[2−4] Cytochrome proteins are mostly associated with Gram-negative bacteria, such as pentahemes from *Wolinella succinogenes*, octahemes from *Nitrosomonas europaea* and decaheme from *Shewanella oneidensis*, which harness energy from the environment during their cycling of N, S, and Fe, with the processes of redox and ET involved.[2] The most prominent examples of such bacteria are *Shewanella oneidensis* and *Geobacter metallireducens*, which are capable of dissimilatory metal-reducing insoluble mineral oxides, such as Fe(III) and Mn(III/IV) oxides,[2,5] by transferring electrons from the interior of the cell to the exterior through multi-*c*-type cytochrome nanowire assembly[6−8] in an anaerobic environment. Besides the unique capability of long-distance ET (up to several micrometers),[2] multiheme cytochromes can perform other remarkable functionalities, including electron storage[9] and redox catalytic activities in enzymes,[2−4] e.g., nitrite reductase, hydroxylamine oxidoreductase, and tetrathionate reductase.

The behavior of monoheme cytochrome *c* when interacting with nanoparticles[10] or electrode surfaces[11] has attracted great attention due to their practical applications in electrochemistry and biotechnologies. Recent studies show that nanohybrid with graphene or carbon nanotube facilitates the separation of photoexcited electron-hole pairs, which can detect nitric oxide[12] and infrared.[11,13] However, the adsorption behavior of multiheme cytochromes on substrate surface and their effects on ET still remain poorly understood. Multiheme cytochromes can form a network of versatile ET pathways to facilitate ET. The studies of multiheme protein's interfacial behavior will open up a new perspective for a variety of applications, including bioenergy,[2] solar-conversion catalyst[14] and the removal of toxic hexavalent chromium from water.[15] In the form of *in situ* electrochemical-based biosensors, the chemo-

Received: December 10, 2015
Accepted: February 17, 2016
Published: February 17, 2016

DOI: 10.1021/acs.jpclett.5b02746
J. Phys. Chem. Lett. 2016, 7, 929−936

physical process typically involves molecular immobilization onto conducting electrodes such as Au and Pt.[16−19] Decaheme cytochrome, MtrF, similar to homologue MtrC, is proposed as *Shewanella oneidensis*' extracellular contact with the substrate surface to facilitate ET. MtrF is folded into four domains: domains I and III mainly consist of β-sheet structures, while domains II and IV are rich in α-helix that is tightly packed with five binding hemes in each domain.[20] Moreover, MtrF surface is covered with multiple sulfur atoms which form possible thio-interactions with a gold substrate surface and thus complicate protein surface diffusive behavior.

To achieve the rational design of biotechnologies involving multiheme cytochromes, the central question is which orientations and structures of the adsorbed protein (particularly the orientations and positions of heme rings) are favorable for ET?[2] Atomistic molecular dynamics (MD) simulation has limitations: the result of protein adsorption is highly dependent on the protein's initial orientation,[21,22] due to large molecular size, slow rotational motion, and possible strong driving forces; moreover, it is highly computationally expensive to perform full-atom MD simulations of macromolecules in explicit water.[23] How to sample enough conformational space in an aqueous environment is a crucial issue when studying protein's interfacial behavior. Previous studies show that protein adsorption is affected by a combination of complex factors, such as surface charge distribution,[24] morphology,[21,22] roughness,[25] surface tension,[26] buffer's ions,[27] and protein surface's heterogeneity in charge and hydrophobicity. Among those factors, electrostatic interactions[24,26] and water-mediated hydrophobic and hydration forces[26,28] have been found to be the most important. The molecular mechanics/Poisson−Boltzmann surface area (MM-PBSA) method has been shown to yield an accurate and efficient estimation[26,29−33] of macromolecular binding free energy, which incorporates protein−surface interactions and hydration or dehydration free energy. Furthermore, MM-PBSA method provides quantitative analysis of thermodynamic driving and barrier forces for protein docking or adsorption. By adopting the predicted adsorption protein structure, subsequently, KMC simulations are performed to study ET across cytochrome protein(s),[34] including the hopping of electrons between Fe atoms, and the injection (i.e., reduction) and ejection (i.e., oxidation) of electrons. To study ET transfer across cytochrome protein complex, we developed a software framework named VizBET, which consists of homology modeling, MD simulation, protein docking, binding free energy computations, KMC simulation of ET dynamics,[35] and the visualization of ET.[36]

As an extension of our previous simulations and experimental work on protein adsorption,[21,22,26,27,37,38] ET across docked protein complex[36] and lipids[39] in an aqueous environment, we used MtrF in this work as a prototypical multiheme protein to study its adsorption and ET on an Au(111) surface in water by using a hybrid simulation scheme: full-atom MD simulation, MM-PBSA method,[26,29−33] and KMC.[36] MD and MM-PBSA were combined to predict protein adsorption. With the predicted adsorbed protein structure, we carried out KMC to simulate the net electron flux through an adsorbed decaheme cytochrome MtrF by using, as input, the sequential heme-to-heme ET rates computed by Breuer et al.[40]

Our simulations of MtrF adsorption and ET on Au (111) surface (12.11 × 11.99 nm^2) were performed with the following protocols. First, homology modeling was built in accordance with our previously established procedure,[36] as illustrated in the Supporting Information (SI), which was based on the published crystal structure of *Shewanella oneidensis* cytochrome c MtrF (pdb code: 3pmq). It should be noted that, as the published structure misses certain residues around both terminals,[20] we added new residues of a different sequence (see SI) based on experimental information provided by our collaborators. In the following discussion (protein domains and secondary structure), we use the residue number according to our new sequence, i.e., Asn26 in this work corresponds to Asn49 in the original crystal structure (pdb code: 3pmq). Second, hybrid MM-PBSA and full-atom MD were employed to predict adsorbed protein configurations at the Au−water interface. MD simulations were performed in NVT ensemble at 298.15 K with Gromacs (version 4.6.5) software package.[41] Charmm27 force field[42] was adopted for the protein and ions, and the SPC water model was used. Different versions[43−45] of peptide−Au surface interactions in an aqueous environment have been recently developed either with or without an explicit term to account for the effect of surface polarization. Both versions of force field parameters were also used for protein adsorption on a Au surface and showed similar results.[46] In this work, to reduce computational load, the Au−protein and Au−water interactions were modeled with Lennard-Jones (LJ) potential,[43,44] which was fitted with experimental surface tension data. No explicit term for Au surface's induced charges on peptide binding is included in these chosen force field parameters. Therefore, we assigned the Au surface atoms with zero charge and their positions were fixed in the simulation according to the force field.[43,44] The protein was assigned with a net charge of −36 e according to the amino residue protonation/deprotonation states and solvated with 36 Na^+ counterions to neutralize the system at pH 7. In MM-PBSA, the protein's solvated configuration obtained from MD is rotated around its center of the mass as a rigid body by a set of Euler angles (ϕ, θ, ψ) with Z-X-Z rotation convention ($0 \le \phi \le 2\pi$; $0 \le \theta \le \pi$; $0 \le \psi \le 2\pi$) . The increment resolution for ϕ is 90° and 15° for both θ and ψ. During rotation, the protein maintains the minimum protein−surface distance of 0.3 nm. To define Euler angles, two vectors were used: $\boldsymbol{\nu}_1$ as the normal vector parallel to the Z-axis from heme10 to heme5, and $\boldsymbol{\nu}_2$ as the horizontal vector (parallel to X-axis) pointing to the direction from heme7 to heme2. Protein was initially aligned with $\boldsymbol{\nu}_1$ and $\boldsymbol{\nu}_2$ overlapping with Z and X axes, respectively. More details about both MD and MM-PBSA simulations are provided in SI. Finally, ET through adsorbed protein was estimated by using KMC simulation[35] (see SI). The ET transfer rate k_{ij} between the neighboring heme i and j sites was calculated by the nonadiabatic rate equation based on the Marcus theory,[47]

$$k_{ij} = \frac{2\pi}{\hbar}\langle |H_{ij}|^2 \rangle \frac{1}{\sqrt{4\pi\lambda k_B T}} \exp\left(-\frac{(\Delta G_{ij} + \lambda)^2}{4\lambda k_B T}\right) \quad (1)$$

where T is temperature, and $\hbar$ and k_B represent the reduced Planck constant and Boltzmann constant, respectively. The reorganization energy λ and the change of the Gibbs free energy ΔG_{ij} were calculated with the QM/MM method[48,49] by Breuer et al.[40,50,51] The electronic coupling matrix element, H_{ij} in the complex was estimated as follows:

$$\langle |H_{ij}|^2 \rangle^{1/2}(r) = A \exp[-\beta(r - r_0)/2] \quad (2)$$

DOI: 10.1021/acs.jpclett.5b02746
J. Phys. Chem. Lett. 2016, 7, 929−936

where r is the edge-to-edge distance between heme i and j, A = 3.77 meV, r_0 = 3.6 Å, and β = 1.65 Å^{-1}.[40,50,51]

In this work, the initial adsorption orientation of solvated MtrF on Au (111) surface was predicted by examining the binding free energy with MM-PBSA in Euler angle space (Figure 1). On the rigid homogeneous gold surface, the rotation by the first Euler angle ϕ, i.e., around the Z-axis normal to the surface, does not incur an appreciable change in the binding free energy. The minimum energy of different ϕ-angles was shown as a function of angles θ and ψ in Figure 2a. When calculating the binding free energy, the protein−surface interactions were taken into account in terms of partial LJ interactions by using Lennard-Jones potential force field.[43,44] The dehydration effects were also included in MM-PBSA free energy computation.[26] In the energy contour map (see Figure 2a), four most possible adsorption orientation areas are identified and a top candidate from each area is selected based on their strong attractive binding free energy, ranging from −494.81 kT to −335.52 kT (see Figure 2a). For the lowest free-energy (i.e., most attractive) configuration (denoted 1 in Figure 2b), structures of turn (Ala277-Cys278, Asp408-Ser409, and Thr416-Glu417) and α-helix (Asn280-Asp282), mainly in domains II and III, are adjacent to the surface. The sulfur atoms in Cys278 and heme5 residue are displaced toward the substrate surface, forming a thio-bonding between Au surface and the protein. The most important observation for this top-ranked orientation is that the residue of heme5 was positioned adjacent to the surface, providing a pathway for ET from the substrate to the outside, while the second and third most-possible configurations (denoted 2 and 3 in Figure 2b) have heme cofactors oriented away from the substrate. The fourth one (denoted 4 in Figure 2b) also has a heme terminal (heme10) oriented toward the surface, which is favorable for ET, though there is about a difference of 159.29 kT compared with configuration 1.

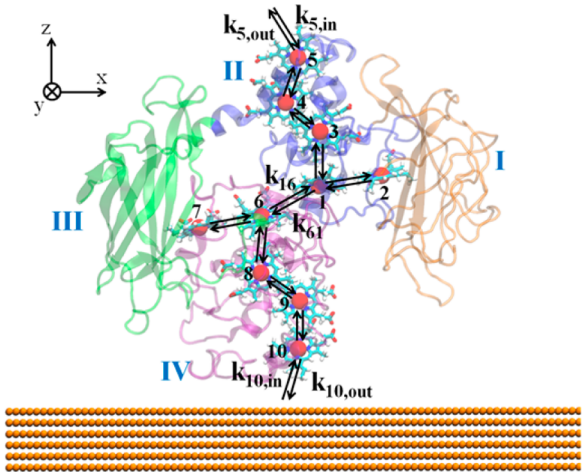

Figure 1. Initial configuration of MtrF for Euler rotation on Au (111) surface (orange) and the electron tunneling path through the heme cofactors (cyan). The protein with four domains was colored sequentially orange, blue, green, and purple from N terminus to C terminus. Iron ions are colored as red balls, whereas the carbon atoms in heme groups are in cyan, the nitrogen in blue, and the oxygen in red. Arrows represent single electron transfer steps from heme i to heme j with reaction rate k_{ji} as well as the ejection/injection steps to/from an external electron acceptor/donor with rate, $k_{i,out}$ and $k_{i,in}$.

To gain more insight into the adsorption driving/barrier force, we itemized the binding free energy into different contributions: protein−surface interactions, ΔE_{LJ} (i.e., Coulombic and LJ interactions), and dehydration of the protein and surface including polar (ΔG_{polar}) and nonpolar ($\Delta G_{nonpolar}$) contributions (see MM-PBSA in the SI). ΔG_{polar} represents water depletion in the long-range governed by water−protein electrostatic interactions, while $\Delta G_{nonpolar}$ refers to water depletion in the short-range (within 0.3 nm), determined by the surface tension and the change of solvent accessible surface area (SASA) for both the protein and substrate surfaces upon adsorption. ΔG_{polar} serves as a barrier force for protein adsorption on the hydrophobic gold surface, whereas $\Delta G_{nonpolar}$ and ΔE_{LJ} are the driving forces. For the attractive

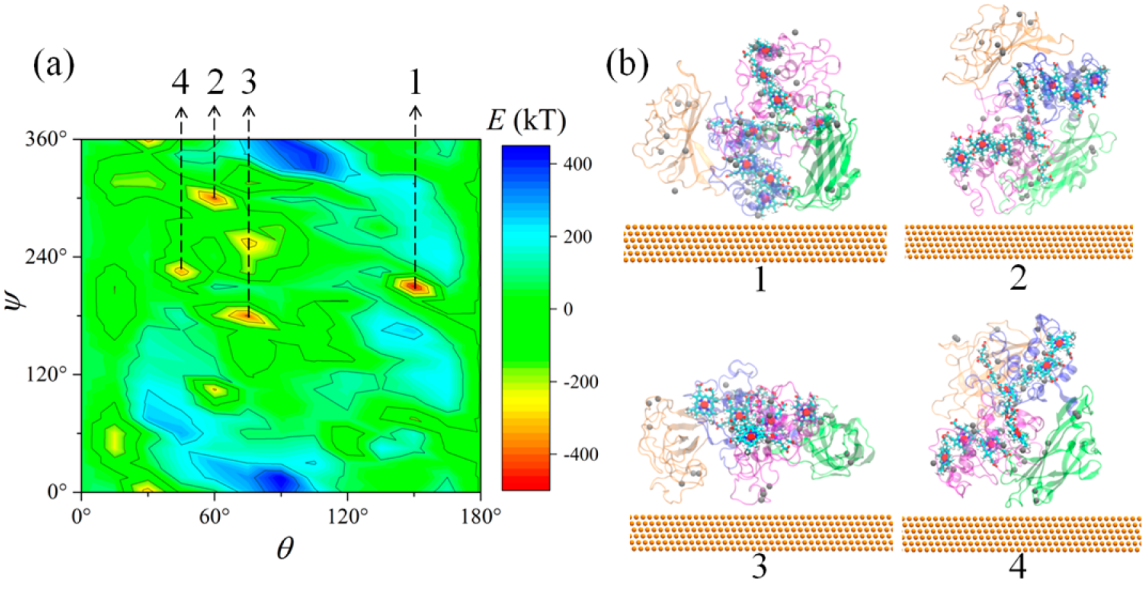

Figure 2. (a) The binding free energy profile of different configurations as a function of the second Euler angle (θ) and third Euler angle (ψ). (b) The four assemblies of energetically most favorable configurations. The binding free energies of the four orientations are −494.81 kT, −403.11 kT, −401.17 kT, and −335.52 kT, respectively. Iron ions, decahemes and sulfur atoms are colored red, cyan and gray, respectively.

DOI: 10.1021/acs.jpclett.5b02746
J. Phys. Chem. Lett. 2016, 7, 929−936

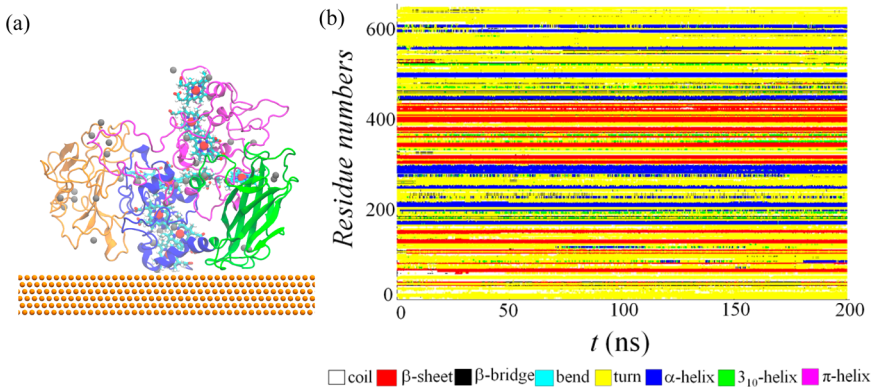

Figure 3. (a) Snapshot of the adsorbed MtrF on Au (111) surface. Water and counterions are not shown for the purpose of clarity. Iron ions, sulfur atoms, and heme cofactors are colored red, gray and cyan, respectively. (b) Time evolution of the secondary structures identified with the method of structural identification (STRIDE).[52]

configurations, the binding free energy is found to be dominated by the nonpolar term, mainly due to the large surface tension of the gold surface (γ_{gold} = 848.82 kJ mol^{-1} nm^{-2}).[43] This result is in agreement with our previous studies, which showed that short-range water depletion plays a major driving force for protein adsorption on hydrophobic surfaces such as graphene or polyethene.[21,22,26] The orientations of rigid β-sheet structures in domains I and III close to the gold surface are found to have less binding free energy (see Figure S3 in the SI). The energetically unfavorable orientations, as shown in Table S1 in the SI, consistently demonstrate smaller nonpolar dehydration energy, indicating that the substrate gold surface is less covered upon protein adsorption. It should also be noted that the protein−Au interactions, i.e., LJ interactions, including thio-reactions, are ∼30% of the short-range dehydration energy for the four most likely configurations in the top-ranking assemblies (see Table S1). No protein−surface electrostatic interaction is taken into account because of the zero-charge of the Au atom according to the force field parameters.[43,44]

MD simulations were carried out in an explicit water environment to further relax the initial configuration (denoted 1 in Figure 2b) of the most attractive binding free energy and the minimum 0.3 nm protein−surface distance in MM-PBSA prediction. Prior to adsorption, the initial solvated structure (snapshot 1 in Figure 2b) shows that domains I (Cys1-Arg163) and III (Ala296-Cys450) are split from the central core (domains II (Asn164-Ser295) and IV(Ala451-His653)). After 210 ns full relaxation, MtrF multiheme electron tunnel terminal, i.e., heme5 in domain II, still remains attached onto the gold surface, and heme10 is exposed to the solvent, which bridges ET through the decaheme MtrF protein between the gold surface and the outside environment. Domain III (Ala296-Cys450) is also attracted to the surface (see Figure 3a and movie1.mp4 in the SI) upon protein adsorption. Aromatic side groups of amide acid residues of Trp283 (in domain II) and Tyr330 (in domain III) attach onto Au(111) surface. Slight structural fluctuation is also observed in domain I. Our observation concurs with the recent literature report,[44] which suggested a "soft epitaxy" mechanism of aromatic-peptide binding on the vacant sites of face-centered cubic lattice above the metal surface. Moreover, the thio-bond between Au surface and sulfur atom of Cys278 in domain II (see Figure 3(a) and movie2.mp4 in the SI) also constrains protein surface mobility. Consequently, the MtrF protein surface motion was suppressed by the protein−surface interaction. Breakage and reformation of strong thio-bonds lead to the protein's intermittent movements on the Au(111) surface, which exhibit highly complex slow dynamics (see movie2.mp4 in SI).

To investigate the effect of image charges of the gold surface, we performed another MD simulation with the same initial configuration, i.e., the most possible configuration predicted from MM-PBSA, by using a different set of force field parameters,[45] which explicitly includes image charges' effect. Our results show no appreciable difference between the two trajectories obtained by using different force field parameters. In addition, we measured surface−protein and surface−water electrostatic energy by using full-atom MD simulations with all the most possible and impossible configurations listed on Table S1, as the input of initial configurations, and by adopting the Au model with dummy dipoles[45] to represent the effect of image charges. The measurements were performed after we relaxed the water molecules and the surface dummy dipole atoms, while fixing positions of all other atoms. It is observed that the ratio between electrostatic energy and Lennard-Jones energy is only about ∼9% (surface−protein) and ∼20% (surface−water either in the bulk water or upon protein adsorption), except one case of the impossible configuration (i.e., listed as item 5 in Table S1) where the surface−protein ratio is up to ∼48%. For the energetic-favorable adsorption configurations, the dominant effect is attributed to Au surface dehydration (see Table S1) due to its large surface energy. In contrast, surface−water electrostatic interactions serve as a barrier force. Therefore, our MM-PBSA search for the most possible orientation to the exclusion of image charges is valid. If the surface's image charges are included in the implementation of Poisson−Boltzmann equations, an accurate dielectric profile of the interfacial region between a protein and Au(111) surface of image charges is needed to estimate the binding free energy. Another alternative way to precisely quantify the contribution of image charges to the total binding free energy is to measure the potential of mean force for protein desorption by using combined full-atom MD in explicit water and umbrella sampling.[38] Further investigation about interfacial dielectric profile as well as the effect of image charges will be discussed in our future work.

With the adsorbed MtrF configuration obtained from the hybrid MM-PBSA and MD simulations with forece field parameters[43,44] without surface image charges, KMC simulations[34−36,53−56] were then performed to study the ET dynamics across the MtrF protein. In KMC, the MtrF protein

DOI: 10.1021/acs.jpclett.5b02746
J. Phys. Chem. Lett. 2016, 7, 929−936

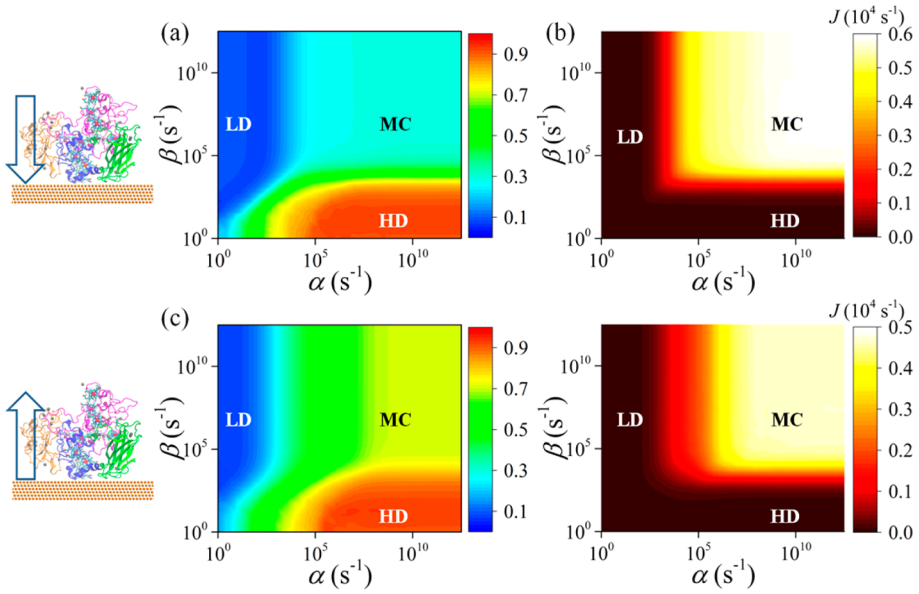

Figure 4. (a,c) Phase diagram of the time-averaged electron occupation density $\langle n \rangle$ for all 10 hemes in adsorbed structure as a function of the incoming (α) and outgoing (β) ET rates for the transfer direction heme10-to-heme5 (from the environment to the surface through the protein) and heme5-to-heme10 (from the surface to the environment through the protein), respectively. (b,d) The corresponding phase diagrams of the net electron flux J of adsorbed protein for the transfer direction heme10-to-heme5 and heme5-to-heme10, respectively.

is treated as a 10-site electron-hopping network, where the heme is labeled by index $i \in [1,10]$ as defined in Figure 1. The ith heme group is either occupied by an electron ($n_i = 1$, corresponding to Fe^{2+}) or unoccupied ($n_i = 0$, corresponding to Fe^{3+}), where n_i is the electron occupation number of the ith heme group. ET across the network is simulated with the electron hopping rate, k_{ij} between adjacent heme pair (i and j), the electron injection rate (α) at the entrance and the ejection rate (β) at the ejection. Here, it should be noted that both injection (α) and ejection (β) rate parameters only refer to an "attempt" rate. The actual injection rate is a product of α and the probability of the electron entrance site being unoccupied; likewise the actual ejection rate is a product of β and the probability of the electron exit site being occupied. For any combination of α and β parameters, KMC simulation converges to a steady state after an initial transient state, where the time-averaged occupation numbers adjust themselves to equate the actual injection and ejection rates. The simulation was initiated with all empty sites in the heme network. The time-averaged electron occupation density at heme i ($\langle n_i \rangle$) was calculated through

$$\langle n_i \rangle = \frac{\sum_{t=1}^{K} n_i(t)\tau(t)}{\sum_{t=1}^{K} \tau(t)} \tag{3}$$

where $n_i(t)$ is the electron occupation number of heme i, and $\tau(t)$ is the time increment at the tth KMC step (see SI). The overall average of the electron occupation density $\langle n \rangle$ is the averaged occupation number of all heme groups. The steady-state current J is defined as the net number of the injection electrons during the KMC steps ($K = 10^6$) divided by the total elapsed time. We used the last six configurations (where each consecutive configuration is separated by 1 ns) to estimate the time-averaged electron occupation density $\langle n \rangle$ and electron flux $\langle J \rangle$.

The study of ET in solid/electrolyte interfaces is fundamental to many electrochemical applications. In bio-sensors,[13] a typical measurement technique is voltammetry (i.e., cyclic voltammetry or ac impedance) in which a negative potential at the working solid electrode is created to induce polarization of charged species and, ultimately, analyte detectability.[19] In this case, the direction of ET going from the electrode to the electrolyte is also commonly known as the cathodic current. In the reverse case, the ET direction flows into the working electrode, creating an anodic current by oxidation of the species in the solvent. This process occurs in applications such as biofuel cells where the working electrode includes redox processes, during which energy can be stored or transferred.[57]

We studied nonequilibrium phase transitions of the heme network as a function of the injection rate (α) and ejection rate (β) from both directions: hem5-to-heme10 (surface-to-environment) and heme10-to-heme5 (environment-to-surface), as shown in Figure 4. As in our previous work,[26] three distinct phases were observed in the time-averaged occupation density of the decaheme MtrF (see Figure 4a,c). When ET is limited by the injection rate from the donors ($\alpha < \beta$) at a low-density (LD) phase, the heme sites are mostly oxidized. By contrast, when ET is limited by the ejection rate to the acceptor ($\alpha > \beta$) at a high-density (HD) phase, the heme sites are mostly reduced. Finally, a "maximum-current" (MC) phase is identified when both α and β rates exceed the smallest intraheme ET rate along the multiheme pathway. For ET of heme10-to-heme5, the rate-limiting step is the intraheme ET from heme10 to heme9 ($\sim 10^3$ s^{-1}), whereas for ET in the reverse direction (i.e., heme5-to-heme10), the rate-limiting step is one of heme6-to-heme8 ($\sim 10^5$ s^{-1}). Figure 4b,d display electron flux in the α–β phase, which has distinct phases (LD, HD, and MC). The electron flux in the direction of heme10-to-heme5 is slightly larger than that in the direction of heme5-to-heme10, due to different driving forces ΔG_{ij} of heme-network along the two directions. We also observed that on the hydrophobic Au (111) surface, ET flux rate across MtrF is lower than that across the structure in the bulk water, i.e., sovlation structure (see Figure

DOI: 10.1021/acs.jpclett.5b02746
J. Phys. Chem. Lett. 2016, 7, 929–936

S5 and Table S2). It should be noted here that the effect of the domain's structural changes on ET transfer parameters based on Marcus' theory require further thorough investigations. The purpose of this work is only to demonstrate the effect of heme-to-heme edge distances through Equation 2 related with electronic matrix elements, H_{ij}, by assuming negligible structural effects. While the magnitude of the electron flux likely depends on the ET parameters used, key features of the nonequilibrium phase diagram involving the low-density, high-density, and maximum-current phases are very robust and are observed in a wide variety of other physical and biological systems. We thus believe that our key findings hold with more accurate estimation of ET parameters.

In summary, we predicted the multiheme cytochrome MtrF adsorption and electron transfer rates on Au (111) surface by using hybrid simulations combining atomistic MD, free energy computing (MM-PBSA), and KMC, while incorporating the dehydration effect and protein−surface thio-interactions. We demonstrated that adsorption orientation, which affects ET through heme network, is mainly controlled by dehydration of the gold surface. Protein−surface thio-interactions also fine-tune the adsorption orientation. The orientation with the heme rings arranged slightly tilted from the surface's normal was predicted to have the most attractive binding free energy, providing an ET pathway from the surface to the solvent environment and vice versa. Protein's secondary structure and domains II and IV are relatively stable during adsorption except for slight movements that are detected on side domain I and III. The constraints from the protein−surface thio-bonding and from strong interactions of peptide aromatic groups and Au(111) surface lead to MtrF protein surface intermittent mobility. More importantly, the ET flux rate across the adsorbed protein of this most energetically favorable orientation was found to be lower than that of the solvated structure. ET flux also varies with the transfer directions. Namely, the electron transfer rate from the surface to solvent via the heme network of the most attractive conformation is smaller than that in the reverse direction. Such atomistic understanding of multiheme cytochrome protein's interfacial behavior can shed light on various biotechnology applications. It is noteworthy that the effect of surface image charges of the water environment[58,59] and peptide-adsorption induced[45,60] on peptide binding have been extensively examined. In our system, the image change effect on the MtrF adsorption is small compared with the dominant effect of Au(111) surface's dehydration.

■ ASSOCIATED CONTENT

Supporting Information

The Supporting Information is available free of charge on the ACS Publications website at DOI: 10.1021/acs.jpclett.5b02746.

The homology modeling of the MtrF protein, the setup of the MD simulation, the mechanics and additional results of the molecular mechanics/Poisson−Boltzmann surface area method, and additional results of kinetic Monte Carlo simulation (PDF)

Movie of the adsorbed MtrF on Au (111) surface (AVI)

Movie showing breakage and reformation of strong thio-bonds leading to protein's intermittent movements on Au(111) surface (AVI)

■ AUTHOR INFORMATION

Corresponding Authors

*E-mail address: twei@lamar.edu.

*E-mail address: anakano@usc.edu.

Notes

The authors declare no competing financial interest.

■ ACKNOWLEDGMENTS

The authors are grateful for insightful discussions on multiheme cytochromes with Dr. Liang Shi (Pacific Northwest National Lab) and Dr. Tom Clarke (University of East Anglia), and on electrochemistry with Dr. Keith Chin (Jet Propulsion Laboratory). The authors are grateful for helpful discussion with Dr. Mohamed Y. El-Naggar (University of Southern California) about MtrF protein. T. Wei thanks the support of computational resources from Texas Advanced Computing Center (TACC), the program of Extreme Science and Engineering Discovery Environment from National Science Foundation (XSEDE/NSF) and Research Enhanced Grant (REG) fund from Lamar University.

■ REFERENCES

(1) Marcus, R. A.; Sutin, N. Electron transfers in chemistry and biology. *Biochim. Biophys. Acta, Rev. Bioenerg.* **1985**, *811*, 265−322.

(2) Breuer, M.; Rosso, K. M.; Blumberger, J.; Butt, J. N. Multi-haem cytochromes in Shewanella oneidensis MR-1: structures, functions and opportunities. *J. R. Soc., Interface* **2015**, *12*, 20141117.

(3) Bewley, K. D.; Ellis, K. E.; Firer-Sherwood, M. A.; Elliott, S. J. Multi-heme proteins: Nature's electronic multi-purpose tool. *Biochim. Biophys. Acta, Bioenerg.* **2013**, *1827*, 938−948.

(4) Mowat, C. G.; Chapman, S. K. Multi-heme cytochromes - new structures, new chemistry. *Dalton Trans.* **2005**, 3381−3389.

(5) Shi, L.; Squier, T. C.; Zachara, J. M.; Fredrickson, J. K. Respiration of metal (hydr)oxides by Shewanella and Geobacter: a key role for multihaem c-type cytochromes. *Mol. Microbiol.* **2007**, *65*, 12−20.

(6) El-Naggar, M. Y.; Finkel, S. E. Live wires. *The Scientist* **2013**, *27*, 38−43.

(7) Pirbadian, S.; Barchinger, S. E.; Leung, K. M.; Byun, H. S.; Jangir, Y.; Bouhenni, R. A.; Reed, S. B.; Romine, M. F.; Saffarini, D. A.; Shi, L.; et al. Shewanella oneidensis MR-1 nanowires are outer membrane and periplasmic extensions of the extracellular electron transport components. *Proc. Natl. Acad. Sci. U. S. A.* **2014**, *111*, 12883−12888.

(8) Leung, K. M.; Wanger, G.; El-Naggar, M. Y.; Gorby, Y.; Southam, G.; Lau, W. M.; Yang, J. Shewanella oneidensis MR-1 bacterial nanowires exhibit p-type, tunable electronic behavior. *Nano Lett.* **2013**, *13*, 2407−2411.

(9) Bauss, A.; Koslowski, T. Storage, transport, release: heme versatility in nitrite reductase electron transfer studied by molecular dynamics simulations. *Phys. Chem. Chem. Phys.* **2015**, *17*, 4483−4491.

(10) Meyer, T.; Gross, J.; Blanck, C.; Schmutz, M.; Ludwig, B.; Hellwig, P.; Melin, F. Electrochemistry of Cytochrome c(1), Cytochrome c(552), and Cu-A from the respiratory chain of thermus thermophilus immobilized on gold nanoparticles. *J. Phys. Chem. B* **2011**, *115*, 7165−7170.

(11) Lai, B. Y.; Chu, C. H.; Su, G. D. J. Long-wavelength infrared sensing by Cytochrome c protein thin film deposited by the spin coating method. *Sensors* **2013**, *13*, 15833−15845.

(12) Wu, J.-F.; Xu, M.-Q.; Zhao, G.-C. Graphene-based modified electrode for the direct electron transfer of Cytochrome c and biosensing. *Electrochem. Commun.* **2010**, *12*, 175−177.

(13) Gong, Y. P.; Liu, Q. F.; Wilt, J. S.; Gong, M. G.; Ren, S. Q.; Wu, J. Wrapping cytochrome c around single-wall carbon nanotube: engineered nanohybrid building blocks for infrared detection at high quantum efficiency. *Sci. Rep.* **2015**, *5*, 11328.

DOI: 10.1021/acs.jpclett.5b02746
J. Phys. Chem. Lett. 2016, 7, 929−936

(14) Bachmeier, A.; Murphy, B. J.; Armstrong, F. A. A multi-heme favoenzyme as a solar conversion catalyst. *J. Am. Chem. Soc.* **2014**, *136*, 12876−12879.
(15) Xafenias, N.; Zhang, Y.; Banks, C. J. Enhanced performance of hexavalent Chromium reducing cathodes in the presence of Shewanella oneidensis MR-1 and Lactate. *Environ. Sci. Technol.* **2013**, *47*, 4512−4520.
(16) Wang, Y.; Zhu, Y.; Liu, Y.; Yang, Y.; Ruan, Q.; Xu, F. An effective gold nanotubes electrode for amperometric biosensor. *J. Nanosci. Nanotechnol.* **2010**, *10*, 8286−8292.
(17) Kashefi-Kheyrabadi, L.; Mehrgardi, M. A. Aptamer-based electrochemical biosensor for detection of adenosine triphosphate using a nanoporous gold platform. *Bioelectrochemistry* **2013**, *94*, 47−52.
(18) Talemi, R. P.; Mashhadizadeh, M. H. A novel morphine electrochemical biosensor based on intercalative and electrostatic interaction of morphine with double strand DNA immobilized onto a modified Au electrode. *Talanta* **2015**, *131*, 460−466.
(19) Seshadri, S.; Chin, K. B.; Buehler, M. G.; Anderson, R. C. Using electrical impedance spectroscopy to detect water in planetary regoliths. *Astrobiology* **2008**, *8*, 781−792.
(20) Clarke, T. A.; Edwards, M. J.; Gates, A. J.; Hall, A.; White, G. F.; Bradley, J.; Reardon, C. L.; Shi, L.; Beliaev, A. S.; Marshall, M. J.; et al. Structure of a bacterial cell surface decaheme electron conduit. *Proc. Natl. Acad. Sci. U. S. A.* **2011**, *108*, 9384−9389.
(21) Wei, T.; Carignano, M. A.; Szleifer, I. Lysozyme adsorption on polyethylene surfaces: why are long simulations needed? *Langmuir* **2011**, *27*, 12074−12081.
(22) Wei, T.; Carignano, M. A.; Szleifer, I. Molecular dynamics simulation of Lysozyme adsorption/desorption on hydrophobic surfaces. *J. Phys. Chem. B* **2012**, *116*, 10189−10194.
(23) Shaw, D. E.; Maragakis, P.; Lindorff-Larsen, K.; Piana, S.; Dror, R. O.; Eastwood, M. P.; Bank, J. A.; Jumper, J. M.; Salmon, J. K.; Shan, Y. B.; et al. Atomic-level characterization of the structural dynamics of proteins. *Science* **2010**, *330*, 341−346.
(24) Chen, S.; Li, L.; Zhao, C.; Zheng, J. Surface hydration: principles and applications toward low-fouling/nonfouling biomaterials. *Polymer* **2010**, *51*, 5283−5293.
(25) Satulovsky, J.; Carignano, M.; Szleifer, I. Kinetic and thermodynamic control of protein adsorption. *Proc. Natl. Acad. Sci. U. S. A.* **2000**, *97*, 9037−9041.
(26) Nakano, C. M.; Ma, H.; Wei, T. Study of lysozyme mobility and binding free energy during adsorption on a graphene surface. *Appl. Phys. Lett.* **2015**, *106*, 153701.
(27) Wei, T.; Kaewtathip, S.; Shing, K. Buffer effect on protein adsorption at liquid/solid interface. *J. Phys. Chem. C* **2009**, *113*, 2053−2062.
(28) Ostuni, E.; Grzybowski, B. A.; Mrksich, M.; Roberts, C. S.; Whitesides, G. M. Adsorption of proteins to hydrophobic sites on mixed self-assembled monolayers. *Langmuir* **2003**, *19*, 1861−1872.
(29) Massova, I.; Kollman, P. A. Computational alanine scanning to probe protein-protein interactions: A novel approach to evaluate binding free energies. *J. Am. Chem. Soc.* **1999**, *121*, 8133−8143.
(30) Srinivasan, J.; Cheatham, T. E.; Cieplak, P.; Kollman, P. A.; Case, D. A. Continuum solvent studies of the stability of DNA, RNA, and phosphoramidate - DNA helices. *J. Am. Chem. Soc.* **1998**, *120*, 9401−9409.
(31) Paissoni, C.; Spiliotopoulos, D.; Musco, G.; Spitaleri, A. GMXPBSA 2.0: A GROMACS tool to perform MM/PBSA and computational alanine scanning. *Comput. Phys. Commun.* **2014**, *185*, 2920−2929.
(32) Paissoni, C.; Spiliotopoulos, D.; Musco, G.; Spitaleri, A. GMXPBSA 2.1: A GROMACS tool to perform MM/PBSA and computational alanine scanning. *Comput. Phys. Commun.* **2015**, *186*, 105−107.
(33) Baker, N. A.; Sept, D.; Joseph, S.; Holst, M. J.; McCammon, J. A. Electrostatics of nanosystems: Application to microtubules and the ribosome. *Proc. Natl. Acad. Sci. U. S. A.* **2001**, *98*, 10037−10041.
(34) Shimojo, F.; Hattori, S.; Kalia, R. K.; Kunaseth, M.; Mou, W.; Nakano, A.; Nomura, K.-i.; Ohmura, S.; Rajak, P.; Shimamura, K.; et al. A divide-conquer-recombine algorithmic paradigm for large spatio-temporal quantum molecular dynamics simulations. *J. Chem. Phys.* **2014**, *140*, 18a529.
(35) Byun, H. S.; Pirbadian, S.; Nakano, A.; Shi, L.; El-Naggar, M. Y. Kinetic Monte Carlo simulations and molecular conductance measurements of the bacterial decaheme Cytochrome MtrF. *ChemElectroChem* **2014**, *1*, 1932−1939.
(36) Nakano, C. M.; Byun, H. S.; Ma, H.; Wei, T.; El-Naggar, M. Y. A framework for stochastic simulations and visualization of biological electron-transfer dynamics. *Comput. Phys. Commun.* **2015**, *193*, 1−9.
(37) Wei, T.; Mu, S. J.; Nakano, A.; Shing, K. A hybrid multi-loop genetic-algorithm/simplex/spatial-grid method for locating the optimum orientation of an adsorbed protein on a solid surface. *Comput. Phys. Commun.* **2009**, *180*, 669−674.
(38) Wei, T.; Sajib, M. S. J.; Samieegohar, M.; Ma, H.; Shing, K. Self-assembled monolayers of azobenzene derivative on silica and their interactions with lysozyme. *Langmuir* **2015**, *31*, 13543−13552.
(39) Arima, Y.; Iwata, H. Effect of wettability and surface functional groups on protein adsorption and cell adhesion using well-defined mixed self-assembled monolayers. *Biomaterials* **2007**, *28*, 3074−3082.
(40) Breuer, M.; Rosso, K. M.; Blumberger, J. Electron flow in multiheme bacterial cytochromes is a balancing act between heme electronic interaction and redox potentials. *Proc. Natl. Acad. Sci. U. S. A.* **2014**, *111*, 611−616.
(41) Hess, B.; Kutzner, C.; van der Spoel, D.; Lindahl, E. GROMACS 4: Algorithms for highly efficient, load-balanced, and scalable molecular simulation. *J. Chem. Theory Comput.* **2008**, *4*, 435−447.
(42) MacKerell, A. D.; Bashford, D.; Bellott, M.; Dunbrack, R. L.; Evanseck, J. D.; Field, M. J.; Fischer, S.; Gao, J.; Guo, H.; Ha, S.; et al. All-atom empirical potential for molecular modeling and dynamics studies of proteins. *J. Phys. Chem. B* **1998**, *102*, 3586−3616.
(43) Heinz, H.; Vaia, R. A.; Farmer, B. L.; Naik, R. R. Accurate simulation of surfaces and interfaces of face-centered cubic metals using 12−6 and 9−6 Lennard-Jones potentials. *J. Phys. Chem. C* **2008**, *112*, 17281−17290.
(44) Heinz, H.; Farmer, B. L.; Pandey, R. B.; Slocik, J. M.; Patnaik, S. S.; Pachter, R.; Naik, R. R. Nature of Molecular Interactions of Peptides with Gold, Palladium, and Pd-Au Bimetal Surfaces in Aqueous Solution. *J. Am. Chem. Soc.* **2009**, *131*, 9704−9714.
(45) Wright, L. B.; Rodger, P. M.; Corni, S.; Walsh, T. R. GolP-CHARMM: First-principles based force fields for the interaction of proteins with Au(111) and Au(100). *J. Chem. Theory Comput.* **2013**, *9*, 1616−1630.
(46) Penna, M. J.; Mijajlovic, M.; Biggs, M. J. Molecular-Level Understanding of Protein Adsorption at the Interface between Water and a Strongly Interacting Uncharged Solid Surface. *J. Am. Chem. Soc.* **2014**, *136*, 5323−5331.
(47) Marcus, R. Chemical and electrochemical electron-transfer theory. *Annu. Rev. Phys. Chem.* **1964**, *15*, 155−196.
(48) Warshel, A.; Levitt, M. Theoretical studies of enzymic reactions: dielectric, electrostatic and steric stabilization of the carbonium ion in the reaction of lysozyme. *J. Mol. Biol.* **1976**, *103*, 227−49.
(49) Warshel, A.; Karplus, M. Calculation of ground and excited state potential surfaces of conjugated molecules. I. Formulation and parametrization. *J. Am. Chem. Soc.* **1972**, *94*, 5612−5625.
(50) Breuer, M.; Zarzycki, P.; Blumberger, J.; Rosso, K. M. Thermodynamics of electron flow in the bacterial deca-heme Cytochrome MtrF. *J. Am. Chem. Soc.* **2012**, *134*, 9868−9871.
(51) Breuer, M.; Zarzycki, P.; Shi, L.; Clarke, T. A.; Edwards, M. J.; Butt, J. N.; Richardson, D. J.; Fredrickson, J. K.; Zachara, J. M.; Blumberger, J.; et al. Molecular structure and free energy landscape for electron transport in the decahaem cytochrome MtrF. *Biochem. Soc. Trans.* **2012**, *40*, 1198−U58.
(52) Frishman, D.; Argos, P. Knowledge-based protein secondary structure assignment. *Proteins: Struct., Funct., Genet.* **1995**, *23*, 566−579.

DOI: 10.1021/acs.jpclett.5b02746
J. Phys. Chem. Lett. 2016, 7, 929−936

(53) Fichthorn, K. A.; Weinberg, W. H. Theoretical foundations of dynamical Monte Carlo simulations. *J. Chem. Phys.* **1991**, *95*, 1090−1096.
(54) Bortz, A. B.; Kalos, M. H.; Lebowitz, J. L. A new algorithm for Monte Carlo simulation of Ising spin systems. *J. Comput. Phys.* **1975**, *17*, 10−18.
(55) Gillespie, D. T. A general method for numerically simulating the stochastic time evolution of coupled chemical reactions. *J. Comput. Phys.* **1976**, *22*, 403−434.
(56) Voter, A. F. Introduction to the kinetic Monte Carlo method. In *Radiation Effects in Solids*; Springer: Dordrecht, The Netherlands, 2007; pp 1−23.
(57) Rabaey, K.; Rozendal, R. A. Microbial electrosynthesis - revisiting the electrical route for microbial production. *Nat. Rev. Microbiol.* **2010**, *8*, 706−716.
(58) Verde, A. V.; Acres, J. M.; Maranas, J. K. Investigating the Specificity of Peptide Adsorption on Gold Using Molecular Dynamics Simulations. *Biomacromolecules* **2009**, *10*, 2118−2128.
(59) Neves, R. S.; Motheo, A. J.; Fartaria, R. P.; Silva Fernandes, F. M. S. Modelling water adsorption on Au (210) surfaces. I. A force field for water−Au interactions by DFT. *J. Electroanal. Chem.* **2007**, *609*, 140−146.
(60) Heinz, H.; Jha, K. C.; Luettmer-Strathmann, J.; Farmer, B. L.; Naik, R. R. Polarization at metal-biomolecular interfaces in solution. *J. R. Soc., Interface* **2011**, *8*, 220−232.

DOI: 10.1021/acs.jpclett.5b02746
J. Phys. Chem. Lett. 2016, 7, 929−936